Hybrid attitude control on-board UWE-4 using magnetorquers and the electric propulsion system NanoFEEP

Alexander Kramer, Philip Bangert, Klaus Schilling
University Würzburg, Computer Science VII: Robotics and Telematics
Am Hubland, Würzburg, Germany; +49 (0)931 31 80511
kramer@informatik.uni-wuerzburg.de

ABSTRACT

Orbit control on-board a 1U CubeSat was not demonstrated in orbit yet and is the technical goal of the UWE-4 mission. For this purpose, the electric propulsion system NanoFEEP was developed by our partners from TU Dresden. Four thruster heads are integrated into the rails of the CubeSat structure. This paper will give an insight into the first activation of an electric propulsion system on-board a 1U CubeSat on 26th February 2019. On the way to orbit control, attitude control capabilities have to be demonstrated in order to direct the thrust vector as desired. The calibration of the attitude determination sensors and first in-orbit attitude control experiments using the magnetorquers are described. We are able to measure the created torque of a thruster using the attitude determination sensors and can thus compute the created thrust. Finally, some lessons learned of the satellite design and operations of the UWE-4 satellite are discussed.

INTRODUCTION

The University Wuerzburg Experimental Satellite 4 (UWE-4) is the fourth CubeSat towards formation flying designed and built with the help of students. On 27th December 2018 the CubeSat was launched into a sun-synchronous low earth orbit at an average altitude of 585 km. During the first weeks, the health status of the satellite was monitored. End of January 2019 the magnetometer and gyroscope sensor was calibrated in-orbit and first tests with the propulsion system could commence. End of February 2019 the UWE-4 satellite could successfully ignite one of its NanoFEEP thrusters, which was to the authors best knowledge the first time an electric propulsion system was activated on a 1U CubeSat. After this milestone the focus of the operations went to the calibration of the sun sensors and the Kalman filter in order to be able to do attitude control experiments and finally orbit control experiments with the CubeSat. These experiments are still on-going.

MISSION OBJECTIVE

The UWE-4 project has several mission goals. The primary mission objective is the education of students from different fields by giving them the chance to do their project work, thesis work and get hands-on experience in the development of a small satellite mission. The technical mission objective is to demonstrate the electric propulsion system NanoFEEP[1] developed by our partners at TU Dresden on-board a 1U CubeSat, characterize it and use it for orbit control purposes. In order to achieve this goal at first attitude control using a vector-pointing controller has to be demonstrated in order to be capable to direct the thrust vector as desired.

SATELLITE DESIGN

The UWE-4 satellite is a 1U CubeSat, which is – as opposed to others – equipped with an electrical propulsion system and depicted in figure 1.
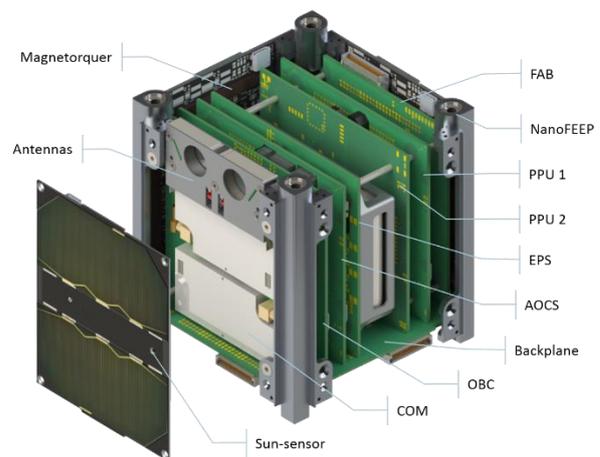

Figure 1: Satellite subsystems of UWE-4.

The satellite is built according to the UNISEC Europe electrical interface standard. It consists of redundant power storage, UHF communication interfaces and on-board computers.

The attitude and orbit control system (AOCS) has access to eight inertial measurement units (IMU) covering three axis gyroscopes, magnetometers and accelerometers. The suite of attitude determination sensors is completed by a novel kind of miniaturized sun-sensor on each of the six side panels. These sun-sensors are pinhole cameras with a resolution of 250 x 250 pixels. During the process of sun recognition, a sun center is found and thus the sun center can be estimated theoretically with sub-pixel resolution.

The side panels also feature a magnetorquer with a maximum magnetic moment of 0.05 Am² each as primary attitude control actuator. The propulsion system consists of four thruster heads, two neutralizers made of carbon nanotubes on the side panels to maintain the

electrical potential of the spacecraft and two power processing units to facilitate the high voltage conversion. The thrusters are integrated into the rails of the Cubesat structure, all facing the same direction. This placement keeps the valuable space at the center of the satellite and the side panels unoccupied and enables to use the propulsion system not only for orbit control, but also for attitude control purposes around two body axes.

ATTITUDE DETERMINATION

In order to estimate the satellite's attitude an isotropic Kalman filter was implemented in order to perform sensor data fusion of the attitude determination sensors. This filter was used already in the previous mission UWE-3[2] and has been adopted from the Tropical Rainfall Measurement Mission[3].

Sensor Calibration

The gyroscope's offset calibration was done by measuring the zero motion offset and resulted in

$$\omega_{Off} = \begin{bmatrix} -2.235 \\ -3.771 \\ 1.512 \end{bmatrix} mrad/_s. \tag{1}$$

The magnetometer calibration is done with acquired on-board data after the launch. For this purpose the magnetometer was sampled for a duration of 7 hours starting on 31st January 2019 11:25:00 UTC.

The magnitude of the magnetometer measurements **B**$_{meas}$ is invariant to rotations of the satellite, and thus the task

is to find a calibrated magnetic field strength **B**$_{calib}$, which matches the reference magnetic field **B**$_{ref}$ computed using the IGRF model[4].
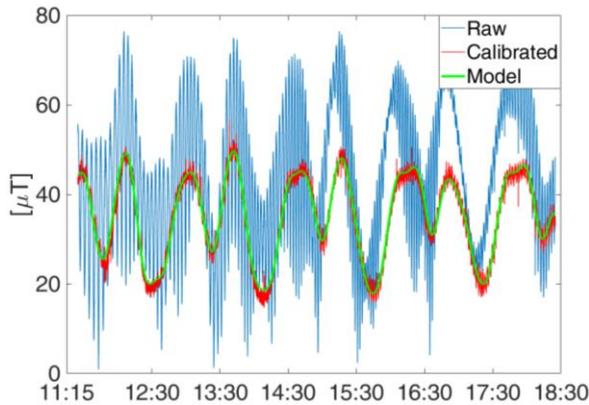

Figure 2: Magnetometer measurement from 31st January 2019.

In a general case a 3x3 calibration matrix **C** and a static offset **µ**$_{Off}$, which satisfies

$$B_{calib} = C * (B_{meas} - \mu_{Off}) \tag{2}$$

and which minimizes the function

$$E = abs(|B_{ref}| - |B_{calib}|) \tag{3}$$

can be found using standard minimization techniques such as the Nelder-Mead Simplex Method[5] used in MATLAB's fminsearch algorithm. At first, this twelve-dimensional minimization (9x**C** + 3x**µ**$_{Off}$) was employed and compared to only six-dimensional (3x**µ**$_{Off}$ + diagonal entries in **C**) and three-dimensional minimization. It resulted in no improvement by the higher dimensional minimizations. Thus, the used IMU allows for the simplification of the matrix **C** to be an identity matrix, since neither cross-axis nor gain effects are present. The used data can be seen in figure 2 and the determined magnetometer offset results to

$$\mu_{Off} = \begin{bmatrix} 14.17 \\ 12.83 \\ -19.44 \end{bmatrix} \mu T. \tag{4}$$

Figure 3 shows the effect of the calibration on the deviation of the measured magnetic field strength to the reference magnetic field, with a resulting standard deviation of 1.34µT.

However, the calibrated data in figure 2 still has a remaining oscillation within the magnetic field data. This oscillation does not vanish with a different calibration, but its amplitude is getting smaller during eclipse and therefore its source is most probably a dynamic magnetic dipole moment, which is being created by e.g. solar cell currents.
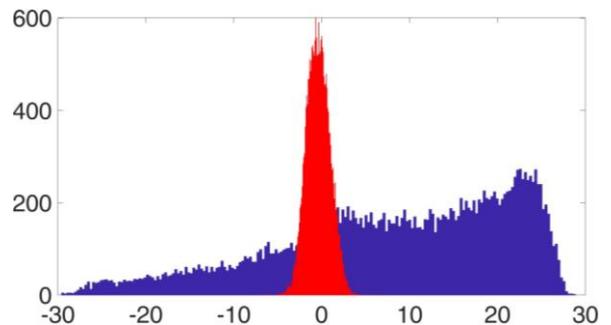

Figure 3: Deviation of the measured magnetic field strength from the reference (IGRF) in µT.

During the very same experiment, also gyroscope data was recorded. Using the method described in Busch et al.[6] a static residual magnetic dipole moment can be roughly determined. Using the Euler equation, the external torque is computed. It is depicted in figure 4 together with the torque created by the static residual external dipole moment, which is in the order of

$$\mu_{res} = \begin{bmatrix} -2.4 \\ 0.1 \\ 0.6 \end{bmatrix} mAm^2. \tag{5}$$

For the calibration measurements of the sun sensors the satellite has been installed on a three axis turntable, which has an angular accuracy of less than 0.4 arcsec[7]. Additionally, a sun simulator providing parallel light was put at about five meters distance to the satellite. The
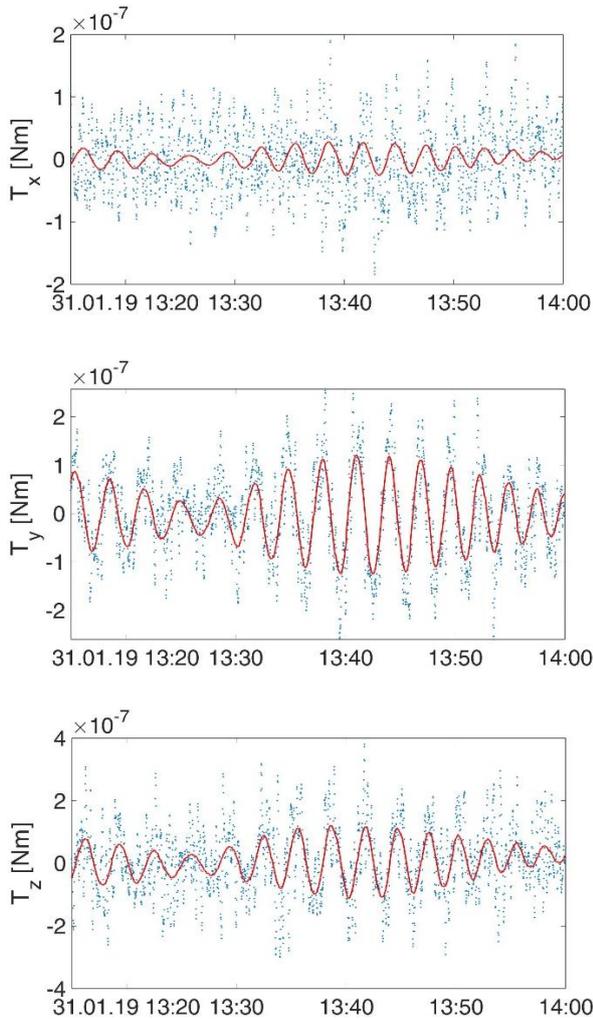

Figure 4: Estimated static residual magnetic dipole torque (red) vs. external torque (blue)

turntable changed the attitude of the satellite relative to the sun simulator in steps of three degrees in a range of ± 30 degrees in two dimensions for each side panel. In every attitude, the center of the light source was determined by the image processing algorithm on the CMOS array, which allowed a calibration of the sun sensors in post-processing.

The image-processing algorithm has several computational steps, which are stated briefly, but are explained in more detail in Chmiela, et al. 2018[8]:

1. At first the center of the sun's image (x,y) on the CMOS array is determined.
2. The pixel coordinates of the sun's center are transformed to a unit vector S_c pointing in the direction of the sun in the sensor frame using a pinhole camera model:

$$S_c = \begin{bmatrix} \dfrac{\sigma_u - x}{a} \\ \dfrac{\sigma_v - y}{b} \\ 1 \end{bmatrix} \tag{6}$$

$$S_c = \frac{S_c}{||S_c||} \tag{7}$$

In formula (6) σ_u & σ_v describe the central pixel which would be determined with vertical incident light. The quantities a and b describe the quotient of focal length and pixel distance in x- and y- direction of the sensor array plane. However, for the used camera this quantities can be assumed to be equal.

3. Subsequently, a fisheye camera model is applied, which has shown an improvement in [8] and is a minor alteration of the previously found sun vector S_c.
4. Finally, the found sun vector is rotated from camera frame into body frame of the satellite.

Thus during the calibration process for each sun sensor several quantities are determined:

- The central pixel coordinates σ_u and σ_v.
- The quotient of focal length and pixel distance a and b.
- The fisheye camera model related quantity x_i.
- The rotation matrix from camera frame to the satellite's body frame.

For reasons of readability the rotation matrices will not be given here, but it can be stated, that the magnitude of rotation is less than ±5° around each panels vertical. The remaining calibration factors are as follows:

Table 1: Calibration factors for the sun sensors

Panel	σ_u	σ_v	a	x_i
+X	111.55	125.23	147.64	0.66
-X	114.10	125.47	149.71	0.66
+Y	117.55	125.71	148.71	0.66
-Y	108.20	125.93	149.88	0.69
+Z	117.57	127.88	106.00	0.26
-Z	112.02	123.41	107.24	0.28

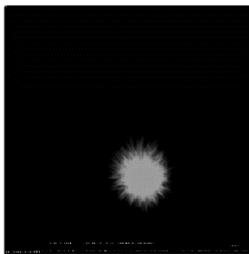The first image of the sun taken with these sun sensors is depicted in figure 5.

Figure 5: First taken sun image on-board UWE-4 on 12th March 2019 with the novel sun sensor on the -Y-panel.
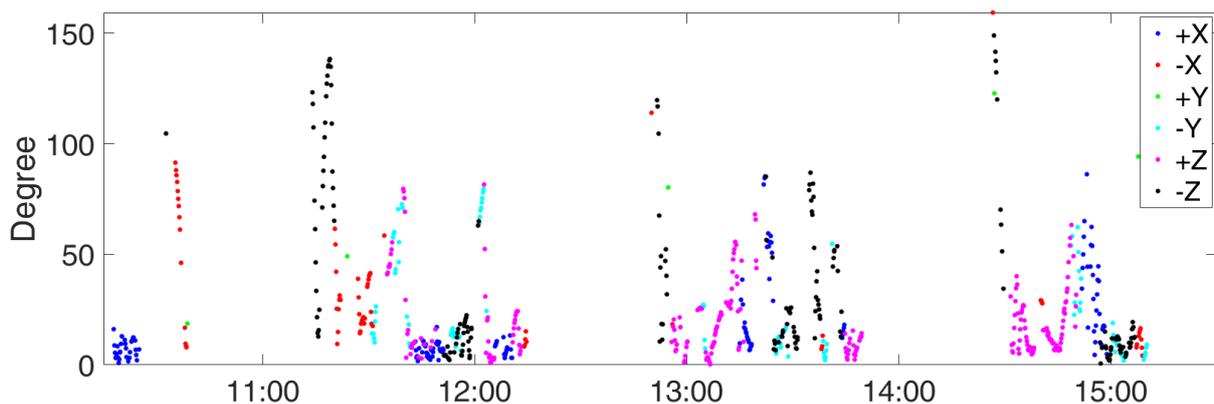
The quality of the calibration shall be assessed by comparing the measured with the reference sun direction. The measured sun direction has to be transformed into the ECI frame using the on-board computed quaternion. For this purpose the measured sun direction as well as the computed quaternions by the Kalman filter have been recorded on 24th May 2019 over a duration of more than three orbits. The error angle between reference sun direction and the measured sun direction is depicted for each sun-sensor in figure 6. It is directly clear that the error is comparably large directly after the eclipse phase of the orbit. Since the Kalman filter, which is estimating the quaternion on-board the satellite, only receives magnetometer inputs during eclipse, this is in line with expectations. However, there are occurrences of no detected sun during the sunlit phase, e.g. during the first orbit around 10:30: UTC. This also leads the Kalman Filter to false estimated quaternions, due to a missing second reference besides magnetometer measurements. The reason for this behavior will be investigated more thoroughly in the future. Additionally, experiments with altered trust levels of the sensor inputs and the model will be conducted. With the known errors, the mean error angle can be calculated for this experiment to 26.6°.

FIRST ACTIVATION OF ELECTRIC PROPULSION SYSTEM ON-BOARD 1U CUBESAT

Prior to the activation of a thruster, it must be ensured that the Gallium propellant has been liquefied. During a sunlit phase this liquefication process may take only a few minutes. However, during the first experiments the propellant solidified during eclipse, where the heater could not provide enough heating power to keep the thruster above 53 °C. An image of a solidification of the propellant, which is an exothermal reaction can be seen in figure 7. It depicts the temperature progression during eclipse on 6th February 2019. With some alterations in the PI-controller of the heater and an ongoing heating

Figure 6: Error angle between measured and reference sun direction.

process over several orbits, no solidification process was observed any more.
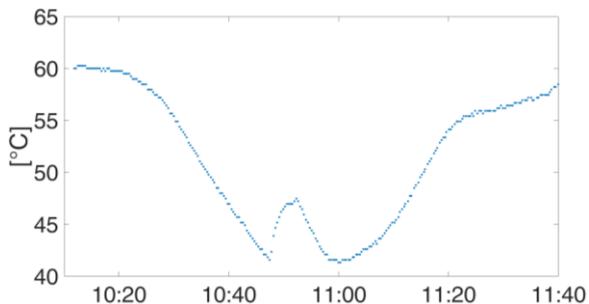

Figure 7: Solidification process of Gallium propellant during eclipse can be seen as exothermal reaction.

The first activation of the electric propulsion system took place on 26th February 2019 09:59:00 UTC after a heating process for at least eight prior orbits. The UWE-4 satellite could successfully ignite one of its NanoFEEP thrusters for a duration of 30s at an operating voltage of more than 5.4 kV and neutralize the emitted charge with an on-board neutralizer. The measurement of the emitted current and the operating voltage of the thruster and the neutralizer is depicted in figure 8. It is necessary that the neutralizer current is never smaller than the thruster current in order to prevent a negative satellite potential from which the satellite could not recover solely by the interaction with the space plasma. Additionally, ions from the thruster just like electrons from the neutralizer may hit the respective extractor electrode and not leave the satellite. These currents were also measured and compensated, but not displayed here for the sake of clarity.

ATTITUDE CONTROL CAPABILITIES

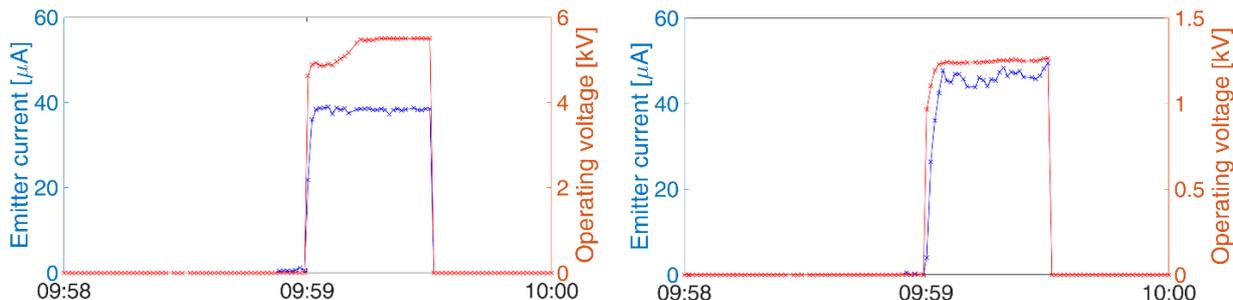The air coils, which are located on each side panel facilitate the creation of a maximum magnetic moment of 0.1 Am^2 per body axis. However, the characteristic of a pure magnetic controller to create only torques perpendicular to the external magnetic field limits the magnetic control capabilities. Additionally, the electric propulsion system can create torques around body x- and y-axis. Thus, it can augment the attitude control capabilities of a pure magnetic controller. Each thruster head contains 0.25 g Gallium as propellant and can create a thrust of up to 20 µN and thus a torque of up to 0.8 µNm.

Magnetic control experiments

On 30th January 2019 a proportional B-Dot controller was activated on-board the AOCS using pure magnetic actuators. Gyroscope as well as magnetometer data was recorded for a duration of more than three hours. The progression of the measured rotation rate is depicted in figure 9. During this time, the satellite detumbled from a rotation rate of about 27 deg/s to less than 5 deg/s. After the first half of the recording the gain of the controller was increased from 0.05 to 0.15. This is also resembled by a faster decrease in the rotation rate.
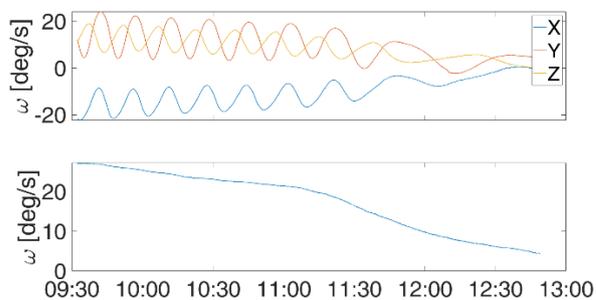

Figure 9: Progression of the rotation rate during detumbling on 30th January 2019. On top the single axes are displayed and on the bottom the absolute value can be seen.

In another recording of a detumbling experiment from 12th February 2019 the behavior at lower rotation rates can be seen nicely. In approximately 100 minutes, the
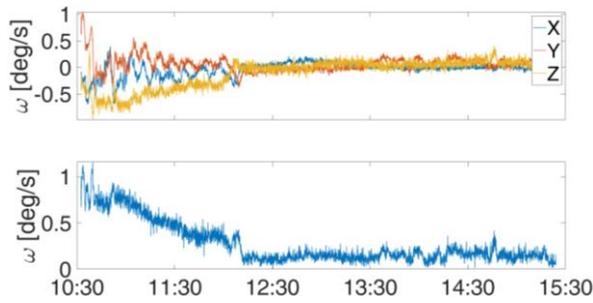

Figure 8: Operating voltage and emitter current of the activated thruster (left) and the respective neutralizer (right).

Figure 10: Detumbling control at low rotation rates below 1 deg/s.

rotation rate declines from 1 deg/s to well below 0.3 deg/s as shown in figure 7.

Initial thruster experiments as attitude control actuator

On 4th May 2019 an initial experiment to the effect of the propulsion system on the satellite's attitude was conducted. For this purpose the thruster located in the +X+Y+Z corner of the CubeSat has been activated with an emitter current of 80 µA and an operating voltage of 6.3 kV. At the same time the neutralizer was operated at more than 1.3 kV to emit an electron current to compensate the thruster current. The effect of the emitted thruster ions on the satellite's rotation rate can be seen in figure 11.
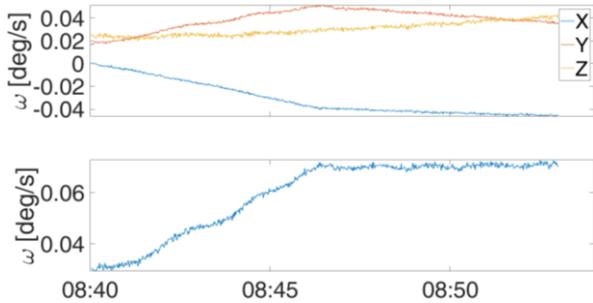

Figure 11: Rotation rate during an activated thruster firing on 4th May 2019.

As visible in figure 12 the thruster was activated between 08:40:11 UTC and 08:46:16 UTC. During this time the rotation rate of the satellite increased from approx. 1.7 deg/s to more than 4.0 deg/s. The electrical characteristics in this figure justify the assumption of a roughly constant emitter current and thus a constantly created thrust.

Using the Euler equation (8) with the derived residual magnetic dipole moment μ_{res} from equation (5) and the moment of inertia matrix I the remaining unexplained external torque M_{ext} acting on the satellite's attitude can be computed.
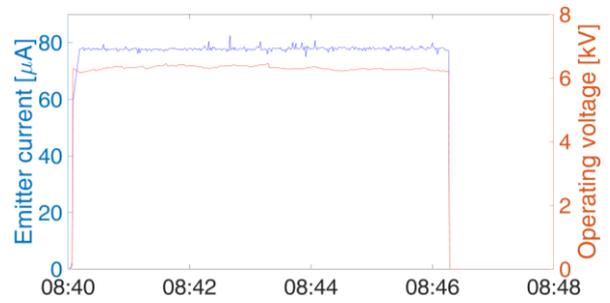

Figure 12: The operating voltage and emitted current of the thruster activated on 4th May 2019.

$$M_{ext} = I\dot{\omega} + \omega \times I\omega - \mu_{res} \times B_{Earth} \qquad (8)$$

A constant thrust F_{Thr} would create a constant torque. Thus minimizing the function

$$E = abs(M_{ext} - r_{Thr} \times F_{Thr}) \qquad (9)$$

with r_{Thr} being the position of the thruster relative to the center of gravity results in a thrust in the range of

$$F_{thr} = -\begin{bmatrix} 0.84 \\ 0.01 \\ 5.23 \end{bmatrix} \mu N. \qquad (10)$$

Figure 13 shows the absolute value of the derived thrust from equation (10) in comparison to the theoretically expected thrust derived from formula (11)[1]:

$$F_{theory} = (I_{emit} - I_{rtn}) * \eta_d$$
$$* \sqrt{2 * m_{Ga} * \frac{U_{Op}}{e}} \qquad (11)$$

In formula 11 I_{emit} describes the emitter current, which has to be reduced by the current I_{rtn}, which is perceived by the extractor and the beam divergence η_d. The atomic mass of the propellant is represented by m_{Ga}, the electron mass by e and the operating voltage of the thruster by U_{Op}.

In theory, the thruster should create a thrust only in –Z direction in the body frame. However, the emitted thruster plume partially hits the satellite's antenna and does therefore create a torque in an undesired direction. Additionally, the antenna may start to oscillate due to the thruster plume and create a torque, which is not reproduced by equation (6). The unknown oscillation in
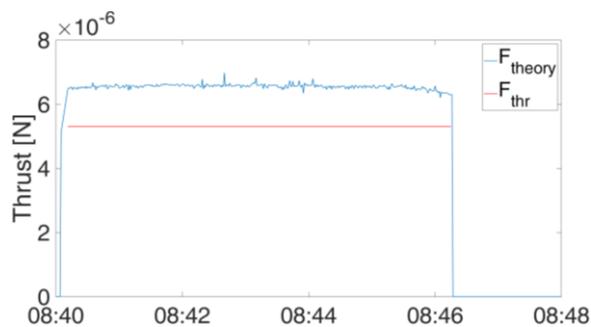
Figure 13: Theoretical thrust (blue) vs. derived thrust from measured rotation rate.

the magnetic field measurements described in the attitude determination chapter also have an influence on the magnetic moment torque in equation (8) and thus restricts the precision of the described analysis method.

LESSONS LEARNED

In the UWE-4 project, there are many learned lessons. However, the focus will be put on the ones, that can be prevented during the design phase of some future mission.

Many educational small satellite projects develop their satellite with the slogan: "Hardware first!" or "Software will be developed as soon as the hardware is delivered to the launch provider". This way of development is possible within some restrictions, because some parts of the satellite still have to be working very flawlessly already during the delivery to the launch provider. In the UWE-4 project, these parts were power generation and storage as well as uplink and software update capability for all subsystems. While other sub-projects like bootstrapping or a general radio communication are also indispensable, the possibility to have a save way for updating the on-board software can save a lot of time during stressful last months before the launch.

However, not putting the focus on radio communication, but trusting on software and hardware fragments from previous missions led to a bad choice in frequency allocation. The initial radio frequency of UWE-4 was at 437.385 MHz. However, this frequency seems to be jammed over Europe[6]. Thus a change of the radio frequency to 435.600 MHz had to be coordinated with the International Amateur Radio Union. While this process was quite rapid, the on-board software update, which facilitates a change of the radio frequency, takes a lot of time, if the success rate at the current frequency is very low.

The sun sensor calibration scheme has been developed for a single sunsensor calibration, because of the lack of

hardware due to production difficulties and a shortage of supplies. However, in the flight model the six sensors have to deliver suitable sun vectors during the hand-over to the sun sensor on a neighboring panel. Unfortunately, it was only possible to do the final calibration measurement for all sun sensors very shortly before the hand-over of the satellite model to the launch provider. This led to measurements that do not cover the whole field of view – only 30° half angle instead of 55° - and also the underlying camera model could have been revised, if the whole satellite model would have been available earlier. Thus, especially for a sensor suite consisting of several sensors covering only a restricted angular space, tests with all sensors in place are essential.

CONCLUSION

A milestone in the 1U CubeSat development was reached with the activation of an electric propulsion system. The attitude determination sensors were calibrated, but the isotropic Kalman filter can still be improved with a proper tuning of its parameters. Initial attitude control experiments with the magnetorquers were conducted and the influence of the thrusters on the satellite's attitude is currently being investigated. In the upcoming weeks, this will result in attitude control experiments with the magnetorquers as main actuators and the thrusters in order to augment the capabilities of the AOCS. Finally orbit control experiments, focusing on a change of the semi-major axis will be conducted.

References

1. Bock, D., Spethmann, A., Trottenberg, T., Kersten, H., and Tajmar, M., „In-plume measurement of NanoFEEP thruster with a force measuring probe using laser interferometry," presented at the 35th International Electric Propulsion Conference, Atlanta, Georgia, USA, 2017.

2. Kiefel, P., Busch, S., Droege, W., and Schilling, K., "Implementation, Calibration and Verification of a Kalman Filter based Attitude Determation System for the Picosatellite UWE-3," GNC 2011, 8th International ESA Conference on Guidance, Navigation and Control Systems.

3. Crassidis, J., Andrews, S., and Markley, F., "Contingency designs for attitude determination of TRMM," Technical report, Goddard Space Flight Center, 1995.

4. Thébault, E. et al., "International Geomagnetic Reference Field: the 12th generation," Earth, Planets and Space, 2015.

5. Lagarias, J.C., Reeds, J.A., Wright, M.H., and Wright, P.E., "Convergence Properties of the Nelder-Mead Simplex Method in Low Dimensions," SIAM Journal of Optimization, Vol. 9, Number 1, 1998.

6. Busch, S., Bangert, P., Dombrovski, S., and Schilling, K., „UWE-3, in-orbit performance and lessons learned of a modular and flexible satellite bus for future picosatellite formations," 65th International Astronautical Congress, Toronto, Canada, 2014.

7. Ruf, O.; Busch, S.; Dombrowski, S.; Schilling, K., "Challenges and Novel Approaches for Testing Large Numbers of Small Satellites," 68th International Astronautical Congress, 2017.

8. Chmiela, K., Bangert, P., Kramer, A., Ziegler, D., Kuhn, T., and Schilling, K., „Development and testing of a high precision sun sensor for the UWE-4 satellite," Master Thesis, Julius-Maximilians-University of Wuerzburg, 2018.